Talanta 271 (2024) 125666

Contents lists available at ScienceDirect

Talanta

journal homepage: www.elsevier.com/locate/talanta

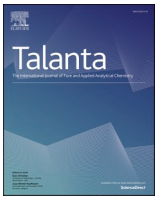

Microwave-sustained inductively coupled atmospheric-pressure plasma (MICAP) for the elemental analysis of complex matrix samples

Raquel Serrano *, Guillermo Grindlay, Luis Gras, Juan Mora

Department of Analytical Chemistry, Nutrition and Food Sciences, University of Alicante, PO Box 99, 03080 Alicante, Spain

ARTICLE INFO

Keywords:
Microwave plasma
Optical emission spectrometry
Metals
Environmental
Food
Polymers

ABSTRACT

Microwave induced plasma optical emission spectrometry (MIP-OES) has gained widespread attention in the last few years for trace elemental analysis. Among the new generation of MIPs it is worth to mention the microwave-sustained inductively coupled atmospheric-pressure plasma (MICAP) for which previous works have shown similar detection capabilities to those afforded by ICP-OES. Nevertheless, this instrument has not been applied yet to complex matrix sample analysis. Therefore, the goal of this work is to evaluate MICAP-OES performance (e.g., analytical figures of merit, matrix effects, etc.) for elemental analysis of samples of different nature (e.g., environmental, food and polymers). To this end, both spectral and non-spectral interferences were investigated for 19 elements (Ag, Al, As, B, Ca, Cd, Co, Cr, Cu, Fe, Ga, In, Mg, Mn, Ni, Pb, Sr, Tl, Zn) in the presence of inorganic acid, organic and saline solutions and compared to a 5 % w w^{-1} HNO_3 solution. Unlike previous MIPs, experimental data showed that the optimum nebulizer gas flow rate for a given emission wavelength was mostly independent of matrix characteristics. Regarding matrix effects, this device was highly robust operating both inorganic acid and organic matrices. Interestingly, when operating saline matrices, changes on emission signal by easily ionizable elements were less significant than those early reported by alternative MIP cavities. Moreover, due to MICAP spectrometer design employed allows real-time simultaneous analysis, Rh, Pd, Sc and Y were suitable internal standards to minimize non-spectral interferences. Finally, MICAP-OES can be successfully applied to the elemental analysis of different complex matrix samples (i.e., CRM-DW1 Drinking water; BCR-146 Sewage sludge industrial; BCR-185 Bovine liver; BCR-278R Mussel tissue; NIST-1549 Non-fat milk powder; ERM-EC681k Polyethylene (high level) and BCR-483 Sewage sludge amended soil).

1. Introduction

Inductively coupled plasma optical emission spectrometry (ICP-OES) is the workhorse technique for trace elemental analysis in many areas due to its outstanding multi-elemental detection capabilities and limits of detection (LoD) at μg L^{-1} levels. Nonetheless, microwave induced plasma optical emission spectrometry (MIP-OES) has been gaining popularity as an alternative technique to ICP-OES for trace element analysis. New instrumental developments (i.e., cavity designs, high-powered magnetrons, etc.) has dramatically improved technique analytical figures of merit, being limits of detection for most metals on a par with those afforded by ICP-OES [1,2]. In addition, one of the most attractive features of current MIP-OES instrumentation is the use of either nitrogen or air for plasma generation, thus reducing significantly operating costs with regard ICP-OES which requires argon instead. Therefore, MIP-OES instruments have been successfully applied for the analysis of samples of very different composition (environmental [3,4], clinical [5], food [6,7], beverages [8], petrochemical [9,10], and ethanol-containing samples [11], among others). For a detailed description of the state-of-the-art readers are referred to the reviews by Muller et al. [1] and Fontoura et al. [2].

Though recent technical advances of MIP-OES, the development of analytical procedures with this technique is still complex since: (i) the nebulizer gas flow (Q_g) affects differently atomic and ionic emission lines which complicates the optimization of the experimental conditions [12,13]; (ii) matrix effects are still significant for samples containing easily ionizable elements (i.e., Na, Ca, Mg, etc.); [14–16]. For instance, signal changes up to 5 and 7-fold have been reported when operating 0.25 mol L^{-1} $NaNO_3$ and 0.25 mol L^{-1} $CaCl_2$ solutions [13] and; (iii) sample throughput is significantly reduced because most instruments make use of sequential spectrometers. Recently, a new MIP cavity design has been developed by Jevtic et al. [17–20] termed

* Corresponding author.
E-mail address: Raquel.serrano@ua.es (R. Serrano).

https://doi.org/10.1016/j.talanta.2024.125666
Received 15 October 2023; Received in revised form 23 December 2023; Accepted 12 January 2024
Available online 14 January 2024

microwave-sustained inductively coupled atmospheric-pressure plasma (MICAP). This new cavity uses a ceramic dielectric resonator ring (Cerawave™) that plays the same role as the traditional ICP load coil. When this device is subjected to a microwave field (2.45 GHz) a magnetic field is generated capable of supporting an annular nitrogen plasma as that obtained with ICPs. Analytical capabilities of this new atomization source have been evaluated for both optical emission (OES) [21–23] and mass spectrometry (MS) [24] providing equivalent analytical figures of merit to those afforded by alternative high-power (N_2)-MIP cavities and argon ICP [22]. Recently, it has been demonstrated that soils [25] and steel [26] samples can be satisfactorily analysed by means of MICAP-MS avoiding the typical Ar-based polyatomic interferences that affect some isotopes (e.g., As, Ca, Cr, Mn, Fe) in ICP-MS. Nevertheless, the feasibility of using MICAP-OES for the analysis of samples with complex matrices have not been reported yet. The lack of technical applications may be attributable to the fact that MICAP has been recently developed and therefore deep-knowledge of matrix effects with this system as well as the appropriate calibration strategies (internal standardization, matrix-matching, standard addition, etc.) to overcome them are limited. It must be considered that even though previous fundamental studies about matrix effects by saline matrices in MICAP-OES have provided a better knowledge of this system [21,27] they cannot be directly extrapolated to routine applications because the concentrations tested are not comparable to those usually employed for real sample preparation [4,13]. Consequently further studies on this regard are required if the MICAP is going to be applied for the analysis of real samples showing complex matrices [13,16].

Thus, the aim of the present study is to evaluate the analytical capabilities of MICAP-OES for trace elemental determination in real sample analysis. To this end, both spectral and non-spectral interferences were systematically investigated for 19 elements (Ag, Al, As, B, Ca, Cd, Co, Cr, Cu, Fe, Ga, In, Mg, Mn, Ni, Pb, Sr, Tl, Zn) in the presence of acid, organic and saline solutions since they are usually employed in sample preparation (digestion and extraction) or even they are naturally present in real samples. Next, the selection of plasma experimental conditions and calibration strategies were examined. Finally, the developed procedure was validated by analysing seven certified reference materials (i.e., environmental, food, and polymers).

2. Experimental

2.1. Reagents

Deionised water produced in a Millipore (Paris, France) Milli-Q device was used to prepare the solutions employed throughout this work. Suprapure nitric acid 69 % w w^{-1}, sulfuric acid 98 % w w^{-1}, hydrochloric acid 37 % w w^{-1}, acetic acid glacial 99.7 % w w^{-1}, calcium chloride 6-hydrate 98 % w w^{-1}, and sodium nitrate 99 % w w^{-1} were purchased from Panreac (Barcelona, Spain). Ethylenediaminetetraacetic acid (EDTA) 98.5 % w w^{-1}, glycerol 86–88 % w w^{-1}, 1000 mg L^{-1} mono-elemental solutions (As, Au, P, Pd, Rh, Sb, Sc, Sn, Ti, V and Y) and 1000 mg L^{-1} multi-elemental ICP-IV solution (Ag, Al, B, Ba, Bi, Ca, Cd, Co, Cr, Cu, Fe, Ga, In, K, Li, Mg, Mn, Na, Ni, Pb, Sr, Tl, and Zn) were obtained from Sigma-Aldrich (Steinheim, Germany).

2.2. Matrix and analyte solutions

Multielemental solutions containing 50 mg kg^{-1} of each analyte (Ag, Al, As, B, Ca, Cd, Co, Cr, Cu, Fe, Ga, In, Mg, Mn, Ni, Pb, Sr, Tl, and Zn) were prepared in six different matrix solutions: (i) 20 g L^{-1} S (prepared from sulfuric acid); (ii) 20 g L^{-1} Cl (prepared from hydrochloric acid); (iii) 20 g L^{-1} C (prepared from glycerol); (iv) 10 g L^{-1} C (equivalent to a 0.43 mol L^{-1} HOAc prepared from acetic acid glacial); (v) 0.10 mol L^{-1} Na (prepared from $NaNO_3$); and (vi) 0.25 mol L^{-1} Ca (prepared from calcium chloride 6-hydrate). For the sake of comparison, a 5 % w w^{-1} nitric acid multielemental solution has been employed as a reference. The concentrations of the solutions were expressed in mol L^{-1} or g L^{-1} unit to facilitate the comparison of the data obtained in the present work with those data previously reported in the literature. Inorganic acids such as sulfuric acid [28] and hydrochloric acid were selected since they are usually employed in sample preparation (e.g., sample storage and acid digestion treatments) [29,30] whereas the use of acetic acid, EDTA and saline matrices in the indicated concentrations were commonly used in different elemental bioavailability extraction methods (e.g., BCR sequential extraction methodology, single-step extraction) [31,32] for the analysis of trace elements in soils and sediments.

2.3. MICAP instrumentation

MICAP-OES measurements were performed using a MICAP-OES 1000 device designed by Radom corporation (Pewaukee, USA), which comprises independent plasma and spectrometer units coupled with a fiber optic connection. The former device consists of an aluminium waveguide that contains a 1.0 kW magnetron to generate the microwave field, an inductive iris to provide impedance matching, the dielectric resonator ring (Cerawave™) and the torch assembly. For all the experiments, a Fassel type quartz torch (20 mm) with a 1.5 mm diameter injector installed vertically (axial view) was used. The sample introduction system employed consisted of a OneNeb® concentric pneumatic nebulizer (Ingeniatrics, Sevilla, Spain) coupled to a cyclonic spray chamber. On the other hand, the spectrometer contains an echelle grating (slit width 30 μm) which allows to simultaneously measure of the entire wavelength range (194–625 nm), and a Peltier-cooled charge-coupled device (sCCD) detector (resolution 2048–2048; pixel size: 11 μm × 11 μm). Instrument operating conditions and emission wavelengths monitored through this work are, respectively, gathered in Table 1 and Table S1 (Supplementary material). The later includes spectroscopic information about analyte atomic and ionic emission lines (i.e. upper electronic level involved in each electron transition, $E_{upper\ level}$) molecular emission bands to assess plasma status (N_2^+ 391.439 nm) and internal standards (Au, Pd, Rh, Sc and Y) used to mitigate potential matrix effects by sample concomitants.

2.4. Samples

To evaluate the strengths and weakness of MICAP-OES for real sample analysis, seven certified reference materials (CRM) were analysed to cover different kind of samples and matrix concomitants (e.g., environmental, food and polymer samples) namely: (i) CRM-DW1 Drinking water; (ii) BCR-146 Sewage sludge industrial; (iii) BCR-185 Bovine liver; (iv) BCR-278R Mussel tissue; (v) NIST-1549 Non-fat milk powder; (vi) ERM-EC681k Polyethylene (high level); and (vii) BCR-483 Sewage sludge amended soil. All samples, except the drinking water and the polyethylene, were oven-dried at 60 °C until constant weight. After that, samples were sieved to <2.0 mm and stored in properly named polyethylene bottles until treatment.

Table 1
MICAP-OES operating conditions.

	MICAP-OES
Plasma forward power (W)	1000
Plasma gas (L min^{-1})	14
Auxiliary gas (L min^{-1})	0.4
Nebulizer gas (Q_g) (L min^{-1})	0.3–0.9
Sample uptake rate (Q_l) (mL min^{-1})	0.3
Sample introduction system:	
Nebulizer	OneNeb®
Spray chamber	Cyclonic (inner volume 42 cm^3)
View mode	Axial
Integration time (s)	1
Replicates	3

2.4.1. Sample digestion

For the determination of the total elemental concentration, the drinking water sample was analysed directly, and the other certified reference materials were digested in triplicate using a Milestone S.r.l. (Sorisole, Italy) Ultrawave oven at conditions recommended by the manufacturer (Table S2). For BCR-146 Sewage sludge industrial, BCR-185 Bovine liver, BCR-278R Mussel tissue and NIST-1549 Non-fat milk powder digestions, 4 mL of HNO_3 65 % w w^{-1} were added to 0.1 g of sample in Teflon vessels, whereas for ERM-EC681k Polyethylene (high level), 4 mL of HNO_3 65 % w w^{-1} and 1 mL of H_2SO_4 98 % w w^{-1} were added to 0.1 g of sample. After the digestion process samples were transferred to polyethylene bottles and brought to a final weight of 15 g with ultrapure water and filtered using a syringe filter of 0.45 μm pore size. Finally, samples were stored at 4 °C until analysis by MICAP-OES.

2.4.2. Extraction procedures

For the elemental bioavailability extraction procedure, the BCR-483 Sewage sludge amended soil was used in four different single step extractions carried out as indicated in Table S3 using the extractions solutions recommended in the CRM report (i.e., 0.05 mol L^{-1} EDTA, 0.43 mol L^{-1} HOAc, 0.01 mol L^{-1} $CaCl_2$ and 0.1 mol L^{-1} $NaNO_3$). After each single step extraction, samples were centrifuged and filtered using a syringe filter of pore size 0.45 μm. Finally, solutions were stored in polyethylene vials at 4 °C until analysis by MICAP-OES.

3. Results and discussion

Analytical capabilities of MICAP-OES in combination with commercially available spectrometers have been previously reported in the literature mainly for some aqueous [23], organic [22] and saline matrices [21,22]. Nevertheless, matrix effects caused by matrices with concentration and composition comparable to those commonly found in sample analysis have not been evaluated yet. Thus, in the present study, three different types of matrices: (i) inorganic acids (i.e., H_2SO_4 and HCl) (ii) organic matrices (i.e., glycerol and acetic acid); and (iii) saline matrices (i.e., Na and Ca concomitants); have been selected to assess spectral and non-spectral interferences. In all cases, a 5 % w w^{-1} nitric acid solution was selected as a reference since it is usually used for sample digestion and conservation and its physicochemical properties are similar to water standards [33]. In this work, a sample introduction system composed by a Oneneb® nebulizer and a cyclonic spray chamber was selected to minimize matrix effects on aerosol generation and transport thus allowing to evaluate the role of the plasma discharge on both spectral and non-spectral interferences [12,13,34]. A plasma power of 1000 W was employed through this work since the MICAP does not allow to modify this parameter. On the other hand, sample uptake rate was fixed at 0.3 mL min^{-1} since there is no signal improvement using higher values (Fig S1). Consequently, the influence of Q_g on both background and analyte emission was specifically investigated.

3.1. Spectral interferences

The background profile and the possible occurrence of additional emission lines and molecular emission bands due to the incomplete atomization of the matrices selected in the plasma were evaluated. The emission profile were monitored in the 194–625 nm wavelength range. Fig. 1 shows the emission spectra obtained at an intermediate Q_g (0.5 L min^{-1}) for each group of matrices (i.e., (A) acid; (B) organic and; (C) saline solutions) along with that obtained for the reference solution, 5 % w w^{-1} nitric acid solution (black line). As expected from previous studies with the MICAP and alternative (N_2)-MIP cavities [22,35], background emission profile for the reference solution was dominated by molecular bands from different nitrogen-based species (Fig. 1A), namely: (i) NO (180–280 nm, B ($^2\Pi$)-X ($^2\Pi$)); (ii) NH (336 nm, A ($^3\Sigma^+$)-X ($^3\Pi$)); and (iii) N_2^+ (390 nm, (B ($^2\Sigma_u^+$)-X ($^3\Sigma_g^+$)) [36]. Non-significant differences in background emission profile were found between

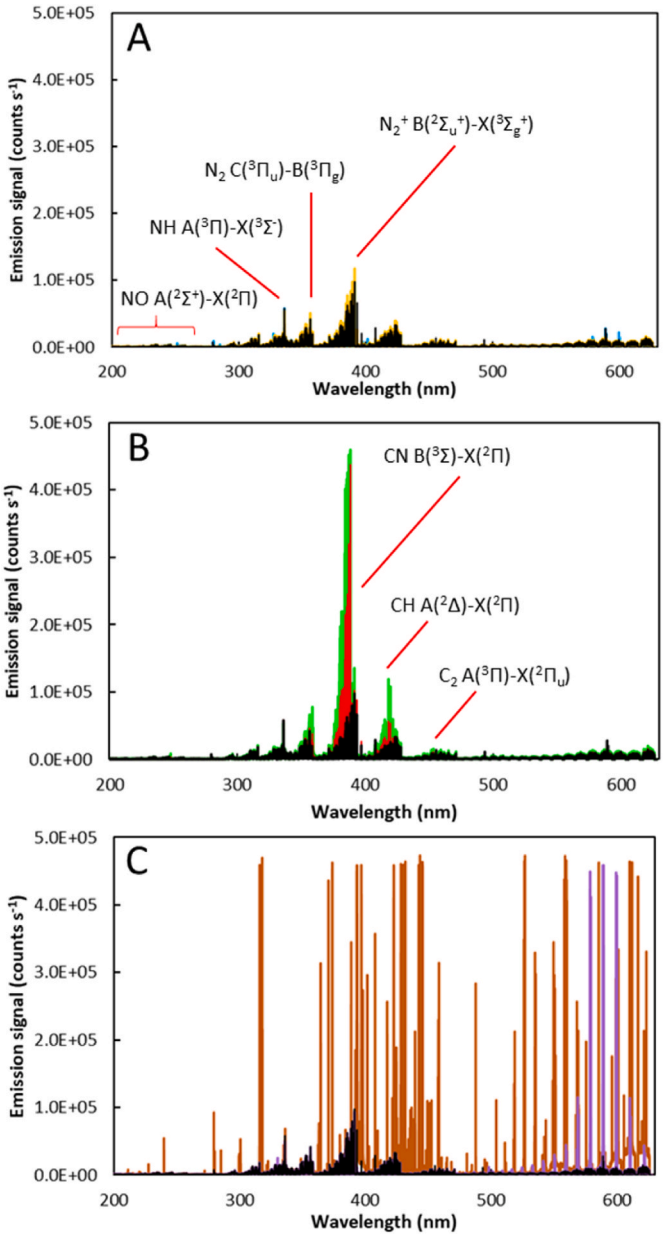

Fig. 1. Background emission profile for (A) inorganic acid (i.e., 20 g L^{-1} Cl (blue) 20 g L^{-1} S (yellow)); (B) organic (i.e., 10 g L^{-1} C (red) and 20 g L^{-1} C (green)); and (C) saline matrices (i.e., 0.25 mol L^{-1} Ca (orange) and 0.10 mol L^{-1} Na (purple)). Background spectrum for the 5 % w w^{-1} nitric acid reference solution is shown in black. Q_g 0.5 L min^{-1}; Q_l 0.3 ml min^{-1}.

inorganic acids (Fig. 1A) and the reference matrix. Additional molecular emission bands and peaks were, however, observed for organic (Fig. 1B) and saline solutions (Fig. 1C). For the former (i.e., 20 g L^{-1} and 10 g L^{-1} C) (Fig. 1B), it is interesting to note, that and increase in the N_2^+ band was noticed. This enhancement was not related to an improvement of N_2 ionization, but mainly due to the spectral interference caused by CN emission band at 388.340 nm (B ($^2\Sigma$)-X ($^2\Pi$)). On this regard, additional carbon-based molecular emission bands appeared at wavelength higher than 388 nm related to other carbon-based molecular species such as CH 431.420 nm (A ($^2\Delta$)-X ($^2\Pi$)) and C_2 473.700 nm (A ($^3\Pi$)-X ($^2\Pi_u$)) [36, 37]. Irrespective of the carbon source employed (i.e., glycerol or acetic acid), carbon-based molecular emission band intensities followed the order CN > CH > C_2. Moreover, as expected from its carbon concentration, the 20 g L^{-1} C solution afforded higher emission signal for the carbon-based molecular species than the 10 g L^{-1} C one. On the other

hand, in the presence of the saline matrices (Fig. 1C) a complex background was recorded for 0.25 mol L^{-1} Ca matrix due to the appearance of different atomic and ionic Ca emission lines [38] as well as to the elemental impurities commonly present in calcium salts (i.e., Sr, Mg, etc.). Similar findings were noticed for the 0.10 mol L^{-1} Na matrix but in these case Na atomic and ionic emission lines were specifically located in the 500–600 nm wavelength range.

Because background emission is strongly correlated to solvent load and plasma characteristics [12], additional experiments were carried out using alternative Q_g values (i.e., 0.3 L min^{-1} - 0.9 L min^{-1}). The results obtained (Fig. S2) shown that, in general, the background emission signal decreased with the increase of Q_g for all the matrices. For instance, operating the 5 % w w^{-1} nitric acid, 20 g L^{-1} S, 20 g L^{-1} Cl, 0.1 mol L^{-1} Na or 0.25 mol L^{-1} Ca at Q_g 0.3 L min^{-1}, the emission signal was 6-fold higher, approximately, than at Q_g 0.9 L min^{-1} in the wavelength range where the main nitrogen molecular emission bands are located (i.e., 300–450 nm). This fact indicates that a greater amount of solvent loaded into the plasma can cause a deterioration of the plasma thermal conditions [12]. Interestingly, in the case of the 0.25 mol L^{-1} Ca solution, as the main emission signal was related to Ca atomic and ionic emission lines, the emission signal increased with the increase of the Qg, since a greater amount of sample, and hence of Ca, reached the plasma. In the case of the organic matrices, for the 20 g L^{-1} C solution the emission signal was only 1.06-fold higher on average at Q_g 0.3 L min^{-1} with respect to that obtained at Q_g 0.9 L min^{-1}. This less noticeable background difference is due to the fact that the emission of the CN molecular band was so strong that it even saturated the detector.

Since the background emission registered for some of the matrices tested was complex, potential spectral interferences could occur on those elements whose most sensitive emission line is located near to molecular emission bands such as: Tm I 384.402, Gd II 385.097, Re I 386.046, Mo I 386.410 nm, Er II 390.631 and Ga I 417.204 nm operating organic solutions, or those lines located above 370 nm (e.g., Sr II 407.771, Ga I 417.104 nm) when a saline solution is introduced in the plasma (Fig. S3).

3.2. Non-spectral interferences

3.2.1. Influence of the nebulizer gas flow rate

It is well known that Q_g plays a significant role on both emission profile and matrix effects in high-power (N_2)-MIP cavities [12,13,37]. Therefore, the influence of Q_g was evaluated for a total of 41 emission lines (atomic and ionic) of 19 elements (Ag, Al, As, B, Ca, Cd, Co, Cr, Cu, Fe, Ga, In, Mg, Mn, Ni, Pb, Sr, Tl, and Zn) in the presence of the matrices selected. Fig. 2 shows the effect of Q_g on the net emission signal of Mn I 279.482 nm and Mn II 257.610 nm for each matrix and the reference solution. These lines were selected to show the different behaviours observed in the presence of the matrices tested. The remaining lines are included in the Supplementary material (Fig. S4). Mn I 279.482 nm emission signal increased up to 0.7 L min^{-1} where a plateau was reached for all the matrices except for 0.25 mol L^{-1} Ca and 0.10 mol L^{-1} Na solutions. For the later matrices, Mn I 279.482 nm emission signal continuously rose up with Q_g (the emission signal increased an 8 % approximately between 0.7 and 0.9 L min^{-1}). In the case of Mn II 257.610 nm, a maximum was observed at a Q_g of 0.5 L min^{-1} for all the matrices tested. Similar findings were registered for the rest of the emission lines evaluated (Table S4). These results indicates that, conversely to that observed for other high-power (N_2)-MIP [12,13], the optimum Q_g for a given wavelength with the MICAP is less affected by matrix characteristics. In general, for MICAP, an optimal Q_g of 0.7 L min^{-1} has been obtained for atomic lines and 0.5 L min^{-1} for the ionic ones, regardless of the matrix considered (Table S4). On the contrary, the data reported by Serrano et al. [12,13] operating a Hammer cavity shown a greater variability between the optimum Q_g values obtained for the different emission lines in the presence of the matrices evaluated. For instance, in that study an optimum Q_g value of 0.6 L min^{-1} was obtained for the Mn II 257.610 nm emission line operating a 5 % w w^{-1} nitric acid whereas the optimum one in the presence of saline solutions (i.e., 0.25 mol L^{-1} Ca and 0.25 mol L^{-1} Na) was 0.4 L min^{-1} [13]. Considering that changes in the emission signal between Q_g 0.5 and 0.7 L min^{-1} were, in general, lower than 10 % for almost all the emission lines tested in the presence of the different matrices evaluated, it is possible to select a compromise value of Q_g to take advantage of the multi-element capabilities offered by MICAP-OES. According to our data, Q_g 0.5 L min^{-1} was selected as a compromise condition to avoid the deterioration of the plasma robustness, and sensitivity according to the data discussed previously (see section 3.1).

Regarding the analyte emission signal, it has been observed that different behaviours could be obtained depending on the characteristics of the lines (i.e., atomic or ionic) and the matrices evaluated. Fig. 2 shown that Mn II 257.610 nm emission signal was negatively affected in the presence of 0.25 mol L^{-1} Ca and 0.1 mol L^{-1} Na, irrespective of the Q_g. For instance, at Q_g 0.5 L min^{-1} the emission signal was supressed approximately 26 and 17 %, with respect to the reference solution, in the presence of 0.25 mol L^{-1} Ca and 0.1 mol L^{-1} Na respectively. On the other hand, for the remaining matrices evaluated changes in the emission signals were between 5 and 8 %, for 10 g L^{-1} C and 20 g L^{-1} S respectively, at Q_g 0.5 L min^{-1} regarding the reference solution. Conversely, Mn I 279.482 nm signal was increased by approximately 41 % in the presence of 0.25 mol L^{-1} Ca and a 17 % approximately with 0.1 mol L^{-1} Na solution regarding the reference solution. Similar behaviours were also obtained for the remaining (atomic and ionic) lines investigated (Fig. S4).

3.2.2. Influence of the emission line characteristics

According to our data as well as previous works in the literature

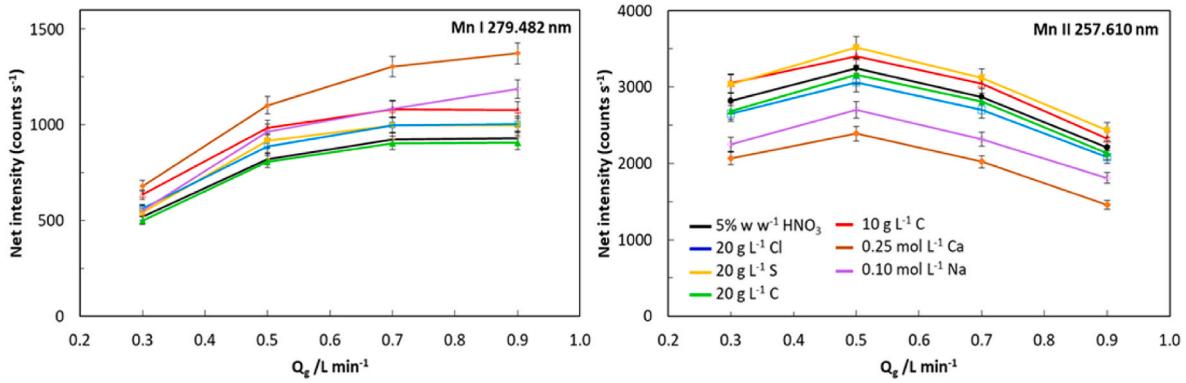

Fig. 2. Influence of the nebulizer gas flow rate (Q_g) on the net emission signal obtained for Mn I 279.482 nm and Mn II 257.610 nm in MICAP-OES operating different matrix solutions.

about non-spectral interferences, it is self-evident that matrix effects on emission signal depends on wavelength characteristics and, more specifically, on the $E_{upper\ level}$ values. For this reason, this matter has been examined in detailed to gain insight into matrix effects origin with the MICAP [13,39]. Fig. 3 shows the influence of the $E_{upper\ level}$ on I_{rel} for the different emission lines selected in the presence of the matrices selected. I_{rel} is defined as the net emission signal of the analyte obtained in each matrix solution relative to that obtained for the 5 % w w^{-1} HNO_3 solution. The signal repeatability for all the lines in the MICAP-OES was, mainly, about 3 % RSD (3 replicates). Hence, it could be considered that

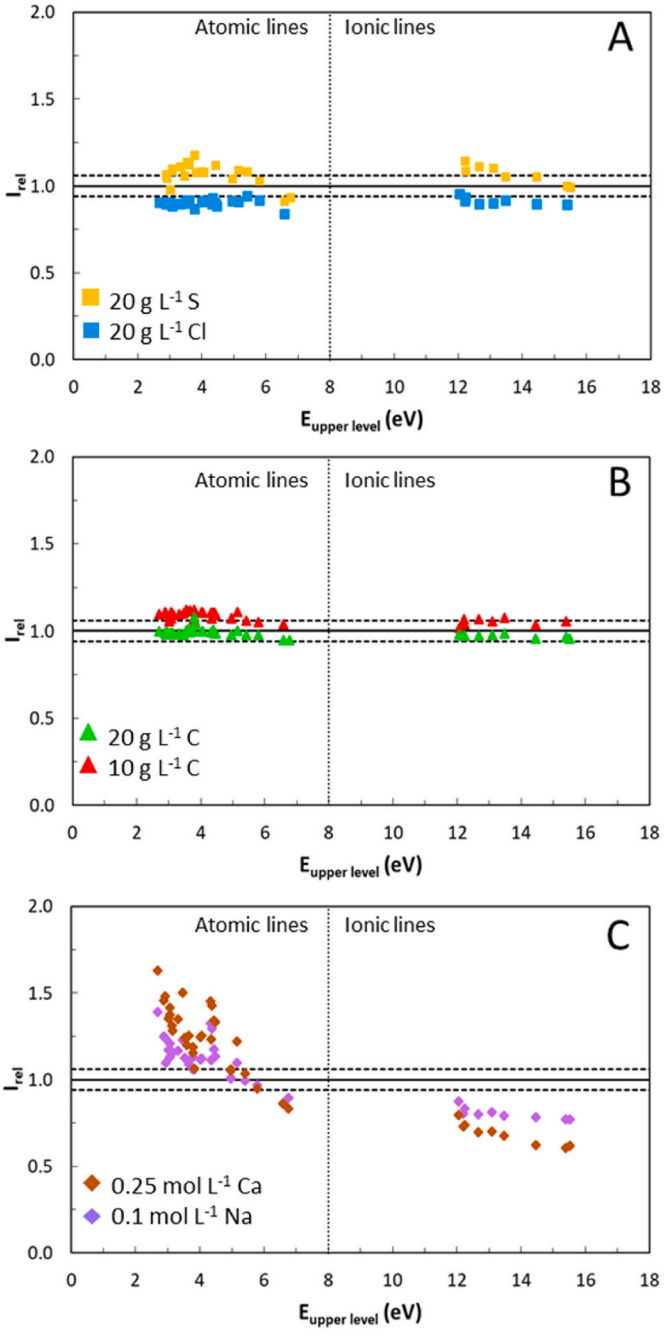

Fig. 3. Influence of $E_{upper\ level}$ on the relative signal intensity (I_{rel}) obtained in the presence of (A) inorganic acid matrices (i.e., 20 g L^{-1} Cl, 20 g L^{-1} S); (B) organic matrices (i.e., 10 g L^{-1} C and 20 g L^{-1} C); and (C) saline matrices (i.e., 0.25 mol L^{-1} Ca and 0.10 mol L^{-1} Na) regarding 5 % w w^{-1} nitric acid. Q_g 0.5 L min^{-1}; Q_l 0.3 ml min^{-1}. I_{rel} values among horizontal dotted lines indicated no matrix effects.

I_{rel} values below 0.94 indicates negative matrix effects (signal suppression) and above 1.06 positive matrix effects (signal enhancement). In general, non-significant matrix effects within experimental uncertainties (dashed lines in Fig. 3) were noticed for the inorganic acid (Fig. 3A) and organic solutions (Fig. 3B). These results are similar to those previously reported for high-power (N_2)-MIP cavities (i.e., Okamoto [14], Hammer [12,13,15,40], MICAP [21], Grand-MP [16]) in the presence of these matrices. On the other hand, for saline matrices (Fig. 3C), it can be observed that I_{rel} values decreased with $E_{upper\ level}$. Interestingly, a cross-over point between positive and negative matrix effects was observed. Atomic lines with $E_{upper\ level} < 4.5$ eV shown positive matrix effects, whereas for atomic lines with higher $E_{upper\ level}$ values and ionic emission lines negative matrix effects ($I_{rel} < 0.94$) prevailed in the presence of both saline matrices (i.e., 0.25 mol L^{-1} Ca and 0.1 mol L^{-1} Na). Moreover, as expected from the salt concentration, the magnitude of the matrix effects was higher for the 0.25 mol L^{-1} Ca solution than for the 0.1 mol L^{-1} Na one. These data contrast with those reported previously by Hallwirth et al. [27] operating alkaline matrices. These authors reported significant matrix effects mainly caused by alkaline elements even at concentration values as low as 20 mg mL^{-1}, but did not observed a correlation between the characteristics of the emission line (i.e., E_{sum}, the sum of the excitation and ionization energy) and the magnitude of matrix effects. These disagreements may be due to the different working conditions and experimental setup used. Thus, both Q_g and Q_l were not specifically optimized and experimental values were selected according to those commonly used in ICP-OES for routine analysis. On the other hand, the nebulizer employed (i.e., Type A, Meinhard, USA) was not the most suitable for the analysis of saline matrices. Nonetheless, the results obtained in the present work agreed with other results reported in the literature for this plasma source [21–23] and alternative high-power (N_2)-MIP cavities [12,13,41,42]. Nevertheless, it is interesting to note that the magnitude of matrix effects registered in this work was lower, for both positive ($I_{rel} > 1.06$) and negative ($I_{rel} < 0.94$) effects, regarding the results reported operating a Hammer cavity using a similar experimental arrangement (i.e., sample introduction system, optimum Q_g and matrix solution composition) [13]. For instance, the I_{rel} values obtained in the present work for the Sr I 460.733 nm ($E_{upper\ level} = 2.69$ eV), which presented positive matrix effects, is 4.3 and 3.4-fold lower for a 0.25 mol L^{-1} Ca and 0.1 mol L^{-1} Na matrices, respectively, with regard the I_{rel} values reported with the Hammer cavity [13]. Conversely, for emission lines affected by negative matrix effects such as Mn II 257.610 nm ($E_{upper\ level} = 12.24$ eV), I_{rel} values are 1.2 and 1.3-fold higher for a 0.25 mol L^{-1} Ca and 0.1 mol L^{-1} Na matrices, respectively operating a MICAP-OES. This fact indicates that MICAP is less prone to non-spectral interferences in the presence of saline solutions than other high-power (N_2)-MIP cavities and, hence, LoDs are less dependent on matrix characteristics. The instrumental LoD values obtained in the presence of some saline matrices employed in elemental bioavailability procedures (i.e., 0.01 mol L^{-1} $CaCl_2$ and 0.1 mol L^{-1} $NaNO_3$) (Table S3) were similar to those obtained for a 5 % w w^{-1} nitric acid matrix (see Table S5). Moreover, it is interesting to note that these LoDs were, in general, of the same order of magnitude as those afforded by both ICP-OES and alternative high-power (N_2)-MIP cavities [22].

To explain experimental findings shown in Fig. 3C, it should be considered how the introduction of saline matrices into the plasma affects the different mechanisms involved in populating atomic and ionic electronic levels (Fig. 4). In the absence of easily ionizable elements (Fig. 4A), ionic levels are populated by N_2^+ and N^+-based charge transfer reactions and the collision with metastable N_2^* species [43,44]. On the other hand, atomic levels are mostly populated by three different mechanisms, namely: (i) electron impact. This excitation pathway affects the low energy atomic levels and depends on both the population of the atom ground level and electronic density; (ii) ion-electron recombination. Unlike the previous mechanism, it affects atomic levels of high energy and depends on both ionic population and electron density; and (iii) collision with metastable atomic N* (^{2}D and ^{2}P levels) species. In

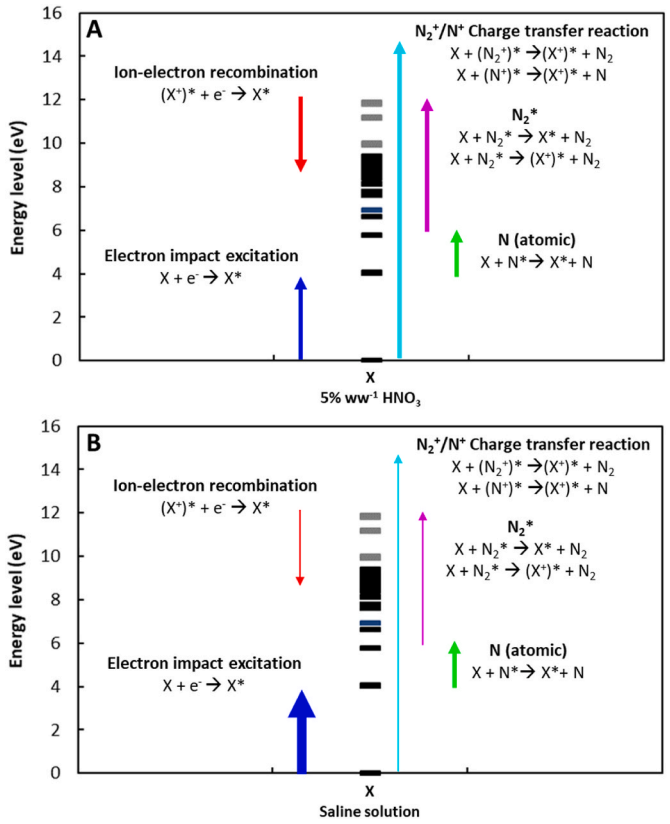

Fig. 4. Simplified atomic (black) and ionic (grey) energy level diagram for an analyte showing potential excitation and ionization pathways operating (A) 5 % w w^{-1} nitric acid and (B) saline solutions. The thickness of the arrows indicates the relevance of the mechanism in each situation.

this case, only atomic levels close to metastable N* (atomic) energy are affected (i.e., 4–5 eV) and it is independent of electron density [44,45]. The introduction of easily ionizable elements into the plasma causes an enhancement in the electron number density affecting a large part of the above-mentioned mechanisms (Fig. 4B) and, hence, both atomic and ionic emission [12,13,21,41,42]. An increase in plasma electron density shifts the ionization equilibrium towards the formation of atoms. This means that the population of analyte (X^+*) and nitrogen (N_2^+ and N^+) ions decrease whereas the atomic ones increase [12,13]. According to this scheme, the signal increase registered for the atomic lines with $E_{upper\ level} < 4.5$ eV can be explained considering that the electron impact mechanism is favored (i.e., higher atomic population and electron density impact). On the other hand, all the mechanisms relying on ionic species (i.e., ion-electron recombination or N_2^+-based charge transfer reactions) are less favored thus affecting negatively the emission signal of both ionic and atomic lines with $E_{upper\ level} > 4.5$ eV. On this regard, because the decrease in the N_2^+ molecular emission band with the MICAP (Fig S5) is lower than that previously reported for the Hammer cavity [12,13] (i.e., emission signal decreased a 48 % and a 80 % in the presence of 0.25 mol L^{-1} Ca solution with regard to the reference solution operating MICAP and Hammer cavity, respectively), it is easier to understand why the magnitude of the matrix effects for the MICAP are lower (i.e., higher plasma robustness). Finally, atomic electronic levels with energy values between 4 and 6 eV are mostly populated by collision with N metastable atoms [46] and they are expected to be less affected by the introduction of easily ionizable elements. In fact, this behavior has also been previously observed in high-power (N_2)-MIP plasmas, regardless the cavity employed [12,13,21,41,42].

3.2.3. Correction of matrix effects

Internal standardization (IS) is a widely employed calibration strategy to mitigate matrix effects and improve analytical figures of merit (e.g., accuracy, precision, long term performance, etc.) in atomic spectrometry. To date, different IS have been successfully proposed for elemental analysis with MIPs, covering either plasma molecular species (the N_2^+ and OH molecular emission band) [47] or elements externally added to both samples and standards (i.e., Te, Co, Be, Ga, In, Sc, Y, etc.) [48,49]. Nevertheless, because sequential spectrometers are usually employed [1,15], this strategy is not easy to apply for multi-elemental determinations since the internal standard and the analytes of interest are not measured simultaneously. For this reason, the purpose of the present study was to evaluate the suitability of five different elements (i.e., Au, Pd, Rh, Sc and Y) as IS, taking advance of the fact that MICAP-OES is equipped with a real-time simultaneous spectrometer. The Au I 242.795, Rh I 369.236 and Pd I 340.458 nm lines were selected as potential IS to correct signal bias for atomic lines whereas Sc II 424.682 and Y II 377.433 nm for the ionic ones.

To evaluate the suitability of the IS, a 5 mg kg^{-1} multielemental solutions containing 0.5 mg kg^{-1} of each IS selected were prepared in two common saline matrices employed in elemental bioavailability procedures (i.e., 0.01 mol L^{-1} $CaCl_2$, 0.1 mol L^{-1} $NaNO_3$) (Table S3) [13] and in 5 % w w^{-1} nitric acid. Table 2 shows the emission signal ratio obtained for different elements and emission lines, selected to cover the $E_{upper\ level}$ range evaluated in previous sections, and the IS in the presence of saline solutions relative to that obtained for the 5 % w w^{-1} HNO_3 solution. As it can be observed, the signal ratio in the presence of both saline solutions was between 0.74 and 1.37 (i.e., an average 1.05 of signal bias) for the analytes and IS emission lines selected, with the exception of Au for which a higher signal bias was obtained (about 50–60 %) for both matrices. This fact may be due to during the preparation of the multielement solutions with the addition of Au, a precipitate appeared. These results were comparable to those reported for similar matrix solutions operating a Hammer cavity instrument equipped with a sequential spectrometer [13]. Hence, Rh, Pd, Sc and Y, could be used in the present work as IS to correct signal bias for atomic and ionic emission lines in the analysis of different CRMs.

3.3. Analysis of complex matrix samples

To evaluate the analytical of capabilities of the MICAP-OES when dealing with complex samples, several CRMs covering a wide range of sample concomitants (i.e., environmental, food, and polymers) were analysed. The CRM-DW1 Drinking water was analysed directly while BCR-146 Sewage sludge industrial, BCR-185 Bovine liver, BCR-278R Mussel tissue, NIST-1549 Non-fat milk powder and ERM-EC681k Polyethylene (high level) materials were analysed after an acid digestion treatment. On the other hand, for the BCR-483 Sewage sludge amended soil four different extractions (i.e., 0.05 mol L^{-1} Na_2EDTA, 0.43 mol L^{-1}

Table 2
Signal ratio obtained for saline solutions (i.e., 0.01 mol L^{-1} $CaCl_2$ and 0.1 mol L^{-1} $NaNO_3$) in comparison with 5 % w w^{-1} nitric acid for a 5 mg kg^{-1} multielemental solution. Q_g 0.5 L min^{-1} and Q_l 0.3 mL min^{-1}.

	Emission line (nm)	$E_{upper\ level}$ (eV)	0.01 mol L^{-1} $CaCl_2$	0.1 mol L^{-1} $NaNO_3$
Analytes	Sr I 460.733	2.69	1.19	1.37
	Cr I 425.435	2.91	0.97	1.18
	Pb I 405.781	4.38	1.01	1.20
	Zn I 213.857	5.80	1.14	0.90
	Mg II 280.271	12.06	1.07	0.84
	Mn II 257.610	12.24	1.08	0.89
	Cd II 226.501	14.46	1.07	0.74
IS	Rh I 369.236	3.36	1.03	1.09
	Pd I 340.458	4.45	n.d.	1.09
	Au I 242.795	5.11	1.56	1.61
	Sc II 424.682	9.79	1.00	0.76
	Y II 377.433	9.97	1.04	0.82

*n.d. not determined.

acetic acid, 0.01 mol L^{-1} $CaCl_2$ and 0.1 mol L^{-1} $NaNO_3$) were performed for the elemental extraction in each soil fraction according to the standardized protocol indicated in the CRM report (Table S3). Sample analysis was carried out using a single set of experimental parameters (i.e., Q_g 0.5 L min^{-1}) and a calibration procedure based on matrix matched standard with Rh and Sc as IS. Method validation was performed according to the European conformity guidelines concerning the performance of analytical methods and the interpretation of results [50] and different international guidance protocols for the analysis of environmental samples [51–53].

3.3.1. Limits of detection

Method limits of detection ($_m$LODs) were estimated according to the IUPAC guidelines [54] using the calibration curve and the most sensitive wavelength of each analyte. The dilution factor (sample mass:final weight) for the sample digestion and the solid:liquid ratio of each extraction procedure were taken into account. It is interesting to note that it was not possible to use the two most sensitive emission lines for Ca (i.e., Ca II 393.366 and Ca II 396.847 nm) in the presence of the 0.43 mol L^{-1} HOAc extraction solution (i.e., 10 g L^{-1} C approximately), since both wavelengths were located near the 380–390 nm range which is interfered by carbon-based molecular emission bands. Thus, the third most intense emission line (Ca I 422.673 nm) was used to estimate the $_m$LODs for this matrix instead. Table 3 gathers the $_m$LODs obtained expressed as mg kg^{-1} dry weight (n = 3) for the different CRMs analysed. In general, $_m$LODs were of the same order of magnitude for all the elements evaluated, except those obtained for the digested CRMs and the 0.43 mol L^{-1} HOAc extraction solution, for which $_m$LODs were one order of magnitude higher. This fact was related to the differences in the dilution factor applied and to the changes in the background signal caused by the presence of carbon. In the case of the analyte Ca, as a less sensitive emission line was used to estimate the $_m$LODs for the 0.43 mol L^{-1} HOAc extraction solution, the value obtained was higher than those obtained for the rest of the extraction solutions, but of the same order of magnitude regarding the $_m$LODs values obtained for the digested CRMs. The $_m$LODs values obtained in this work were similar to those reported operating alternative high-power (N_2)-MIP cavities with solutions of similar composition, especially those obtained for the BCR-483 Sewage sludge amended soil were of the same order of magnitude that those previously reported operating a Hammer cavity [13,55,56].

3.3.2. Trueness

Table 4 shows elemental recoveries for those elements analysed in the different CRMs. In accordance with different international guidance protocols, [54,55,56,57] the accuracy of the measurements of a CRM is successfully assessed when the deviation of the analyte concentration values determined experimentally and those certified for each CRM not lie outside the limit ± 10 %. As it can be observed, in general, quantitatively recovery values (between 90 and 110 %) were obtained for all the analytes tested irrespective of the CRM considered, with the exception of the BCR-483 Sewage sludge amended soil. For this CRM, recovery values outside ±10 % range were obtained for Cr and Zn in the EDTA and $CaCl_2$ extraction solutions, respectively. Lastly, it is interesting to note that concentration values for all the analytes evaluated in the $NaNO_3$ extraction fraction could not be registered due to their low concentration levels.

3.3.3. Precision and robustness

To evaluate the repeatability of the methods tested (intra-day precision), six replicates of each sample were analysed on the same day. For each element, the relative standard deviation (RSD%) varied between 1 and 6 % depending on the CRM. Finally, as regards the reproducibility (inter-day precision), it was evaluated analysing five replicates of each sample in four different days, and it was lower than 8 % for all the samples tested.

4. Conclusions

This work shows that MICAP-OES is a suitable system for the elemental analysis of complex matrix samples. Unlike other high-power (N_2)-MIP cavities (i.e., Okamoto, Hammer, Grand-MP), plasma optimization is more straightforward since, irrespective of the emission line and matrix characteristics, a single Q_g can be selected for the simultaneous analysis of different elements. On the other hand, it has been observed that this system provides a more robust discharge. Irrespective of the emission line considered, no matrix effects were observed when operating acid and organic solutions. Even though this system is still prone to matrix effects caused by easily ionizable elements, changes on both atomic and ionic emission are significantly lower than those traditionally reported for microwave plasmas. In any case, non-spectral interferences by sample concomitants, could be appropriately addressed by means of real-time internal standardization and without compromising sample throughput. Our data shows that there is not a universal IS to correct matrix effects and improve long-term performance thus requiring two internal standards to correct matrix effects for atomic (i.e., Rh or Pd) and ionic (i.e., Sc and Y) emission lines.

CRediT authorship contribution statement

Raquel Serrano: Investigation, Methodology, Project administration, Visualization, Writing – original draft, Writing – review & editing. **Guillermo Grindlay:** Conceptualization, Methodology, Project

Table 3
Method limits of detection ($_m$LODs) expressed as mg kg^{-1} dry weight (n = 3) in MICAP-OES for the different CRMs evaluated. Q_g 0.5 L min^{-1} and Q_l 0.3 mL min^{-1}.

Matrices	CRM-DW1 Drinking water	Digested CRMs	BCR-483 Sewage sludge amended soil			
			0.43 mol L^{-1} HOAc	0.10 mol L^{-1} $NaNO_3$	0.05 mol L^{-1} EDTA	0.01 mol L^{-1} $CaCl_2$
Cr 425.435	0.05	3	2	0.13	0.7	1
Al 396.152	0.04	5	1.2	0.15	0.03	0.15
Ni 352.454	0.08	20	1.3	0.15	1.2	2
Ag 328.068	0.17	90	2	0.53	8	n.d.
Cu 324.754	0.01	9	0.2	0.05	1.0	0.4
Pb 405.781	0.01	12	5	0.25	0.9	1.2
Cd 228.802	0.01	2	1.2	0.25	0.3	0.3
Zn 213.587	0.01	7	1	0.25	0.2	0.6
Ba 493.408	0.01	2	0.3	0.05	0.4	0.3
Ca 393.366	0.05	1	3[a]	0.07	0.6	n.d.
Mg 280.270	0.01	1	1.4	0.03	0.2	0.9
Mn 257.610	0.02	3	0.7	1.00	0.1	0.2
Fe 259.940	0.03	2	1	0.18	0.1	0.2
Co 238.892	0.03	13	10	1.50	0.4	1.7

n.d.: not determined.
[a] LoD value calculated for the emission line 422.673 nm.

Table 4
Analyte percent recoveries (mean ± SD, n = 3) obtained for the different certified reference materials analysed by MICAP-OES. Q_g 0.5 L min^{-1} and Q_l 0.3 mL min^{-1}.

Elements	CRM-DW1 Drinking water	BCR-146R Sewage sludge industrial	BCR-185R Bovine Liver	BCR-278R Mussel tissue	NIST-1549 Non-fat milk powder	ERM-EC681k Polyethylene (high level)	BCR-483 Sewage sludge amended soil		
							EDTA	HOAc	$CaCl_2$
Ca	82.6 ± 1.2	–	–	–	90 ± 3	–	–	–	–
Cd	< LoDs	90 ± 20	< LoDs	< LoDs	< LoDs	90 ± 2	98.8 ± 0.7	88 ± 4	< LoDs
Cr	< LoDs	92 ± 7	–	< LoDs	< LoDs	< LoDs	170 ± 15	92 ± 2	< LoDs
Cu	102 ± 4	91 ± 4	89 ± 2	< LoDs	< LoDs	–	90 ± 4	98 ± 5	< LoDs
Fe	111 ± 5	–	–	–	< LoDs	–	–	–	–
Mg	112 ± 3	–	–	–	92 ± 12	–	–	–	–
Mn	< LoDs	87 ± 4	101 ± 3	95 ± 6	< LoDs	–	–	–	–
Na	103.7 ± 0.2	–	–	–	102.35 ± 0.11	–	–	–	–
Ni	< LoDs	< LoDs	–	–	–	–	106 ± 5	< LoDs	< LoDs
P	–	–	–	–	109 ± 5	–	–	–	–
Pb	< LoDs	91 ± 6	< LoDs	< LoDs	< LoDs	108 ± 10	85 ± 9	< LoDs	< LoDs
Zn	< LoDs	103 ± 5	96 ± 3	98.5 ± 1.5	113 ± 17	101 ± 2	94 ± 2	98 ± 5	145 ± 1

administration, Supervision, Validation, Visualization, Writing – review & editing. **Luis Gras:** Investigation, Methodology, Project administration, Supervision, Validation, Visualization, Writing – review & editing. **Juan Mora:** Funding acquisition, Supervision, Visualization, Writing – review & editing.

Declaration of competing interest

The authors declare that they have no known competing financial interests or personal relationships that could have appeared to influence the work reported in this paper.

Data availability

Data will be made available on request.

Acknowledgements

This research was funded by the University of Alicante through research projects VIGROB-050.

Appendix A. Supplementary data

Supplementary data to this article can be found online at https://doi.org/10.1016/j.talanta.2024.125666.

References

[1] A. Muller, D. Pozebon, V.L. Dressler, Advances of nitrogen microwave plasma for optical emission spectrometry and applications in elemental analysis: a review, J. Anal. At. Spectrom. 35 (2020) 2113–2131.
[2] B.M. Fontoura, F.C. Jofré, T. Williams, M. Savio, G.L. Donati, J.A. Nóbrega, Is MIP-OES a suitable alternative to ICP-OES for trace elements analysis? J. Anal. At. Spectrom. 37 (2022) 966–984.
[3] V. Sreenivasulu, N.S. Kumar, V. Dharmendra, M. Asif, V. Balaram, H. Zhengxu, Z. Zhen, Determination of boron, phosphorus, and molybdenum content in biosludge samples by microwave plasma atomic emission spectrometry (MP-AES), Appl. Sci. 7 (2017) 264–273.
[4] F.C. Jofré, M. Perez, N. Kloster, M. Savio, Analytical methods assessment for exchangeable cations analysis in soil: MIP OES appraisement, Commun, Soil. Sci. Plant 51 (2020) 2205–2214.
[5] E. Baranyai, C.N. Tóth, I. Fábian, Elemental analysis of human blood serum by microwave plasma – Investigation of the matrix effects caused by sodim using model solutions, Biol. Trace Elem. Res. 194 (2020) 13–23.
[6] C.B. Williams, T.G. Wittmann, T. McSweeney, P. Elliott, B.T. Jones, G.L. Donati, Dry ashing and microwave-induced plasma optical emission spectrometry as fast and cost-effective strategy for trace element analysis, Microchem. J. 132 (2017) 15–19.
[7] N. Ozbek, H. Tinas, A.E. Atespare, A procedure for the determination of trace metals in rice varieties using microwave induced plasma atomic emission spectrometry, Microchem. J. 144 (2019) 474–478.
[8] D.A. Goncalves, T. McSweeney, M.C. Santos, B.T. Jones, G.L. Donati, Standard dilution analysis of beverages by microwave-induced plasma optical emission spectrometry, Anal. Chim. Acta 909 (2016) 24–29.
[9] S.M. Azcarate, L.P. Langhoff, J.M. Camiña, A green single-tube sample preparation method for wear metal determination in lubricating oil by microwave induced plasma with optical emission spectrometry, Talanta 95 (2019) 573–579.
[10] J. Nelson, G. Gilleland, L. Poirier, D. Leong, P. Hajdu, F. Lopez-Linares, Elemental analysis of crude oils using microwave plasma atomic emission spectroscopy, Energy fuels 29 (2015) 5587–5594.
[11] T.L. Espinoza Cruz, M. Guerrero Esperanza, K. Wrobel, E.Y. Barrientos, F. J. Acevedo Aguilar, K. Wrobel, Determination of major and minor elements in Mexican red wines by microwave-induced plasma optical emission spectrometry, evaluating different calibration methods and exploring potential of the obtained data in the assessment of wine provenance, Spectrochim. Acta B 164 (2020) 105754.
[12] R. Serrano, G. Grindlay, L. Gras, J. Mora, Evaluation of calcium-, carbon- and sulfur-based non-spectral interferences in high-power MIP-OES: comparison with ICP-OES, J. Anal. At. Spectrom. 34 (2019) 1611–1617.
[13] R. Serrano, E. Anticó, G. Grindlay, L. Gras, C. Fontàs, Determination of elemental bioavailability in soils and sediments by microwave induced plasma optical emission spectrometry (MIP-OES): matrix effects and calibration strategies, Talanta 240 (2022) 123166.
[14] Z. Zhang, K. Wagatsuma, Effects of easily ionizable elements and nitric acid in microwave-induced nitrogen plasma atomic emission spectrometry, Spectrochim. Acta, Part B 57 (2002) 1247–1257.
[15] C.B. Williams, R.S. Amais, B.M. Fontoura, B.T. Jones, J.A. Nóbrega, G.L. Donati, Recent developments in microwave-induced plasma optical emission spectrometry and applications of a commercial Hammer-cavity instrument, Trends Anal. Chem. 116 (2019) 151–157.
[16] E.V. Polyakova, Y.N. Nomerotskaya, A.I. Saprykin, Effect of matrix elements and acid on analytical signals in nitrogen microwave-plasma atomic emission spectrometry, J. Anal. Chem. 75 (2020) 474–478.
[17] J. Jevtic, A. Menon, V. Pikelja, PCT/US2014/024312, WO2014159590 A2014159591, World Intellectual Property Organization, 2014.
[18] J. Jevtic, A. Menon, V. Pikelja, PCT/US2014/024306, WO2014159588 A2014159581, World Intellectual Property Organization, 2014.
[19] J. Jevtic, A. Menon, V. Pikelja, in: Presented at SCIX, Milwaukee, WI, 2013.
[20] J. Jevtic, A. Menon, V. Pikelja, in: Presented at ICOPS/BEAMS 2014, Washington, DC, 2014.
[21] K.M. Thaler, A.J. Schwartz, C. Haisch, R. Niessner, G.M. Hieftje, Preliminary survey of matrix effects in the microwave-sustained, inductively coupled atmospheric-pressure plasma (MICAP), Talanta 180 (2018) 25–31.
[22] A.J. Schwartz, Y. Cheung, J. Jevtic, V. Pikelja, A. Menon, S.T. Ray, G.M. Hietje, New inductively coupled plasma for atomic spectrometry: the microwave-sustained, inductively coupled, atmospheric-pressure plasma (MICAP), J. Anal. At. Spectrom. 31 (2016) 440–449.
[23] H. Wiltsche, M. Wolfgang, Merits of microwave plasmas for optical emission spectrometry – characterization of an axially viewed microwave-sustained, inductively coupled, atmospheric-pressure plasma (MICAP), J. Anal. At. Spectrom. 35 (2020) 2369–2377.
[24] M. Schild, A. Gundlach-Graham, A. Menon, J. Jevtic, V. Pikelja, M. Tanner, B. Hattendorf, D. Günter, Replacing the argon ICP: nitrogen microwave inductively coupled atmospheric-pressure plasma (MICAP) for mass spectrometry, Anal. Chem. 90 (2018) 13443–13450.

[25] Z. You, A. Akkus, W. Weisheit, T. Giray, S. Penk, S. Buttler, S. Recknagel, C. Abad, Multielement analysis in soils using nitrogen microwave inductively coupled atmospheric-pressure plasma mass spectrometry, J. Anal. At. Spectrom. 37 (2022) 2556–2562.
[26] A. Winckelmann, J. Roik, S. Recknagel, C. Abad, Z. You, Investigation of matrix effects in nitrogen microwave inductively coupled atmospheric pressure plasma mass spectrometry (MICAP-MS) for trace element analysis in steels, J. Anal. At. Spectrom. 38 (2023) 1253–1260.
[27] F. Hallwirth, M. Wolfgang, H. Wiltsche, Matrix effects in simultaneous microwave induced plasma optical emission spectrometry: new perspective on an old problem, J. Anal. At. Spectrom. 38 (2023) 1682–1690.
[28] J. Entwisle, R. Hearn, Development of an accurate procedure for the determination of arsenic in fish tissues of marine origin by inductively coupled plasma mass spectrometry, Spectrochim. Acta B 61 (2006) 438–443.
[29] E.M. Seco-Gesto, A. Moreda-Piñeiro, A. Bermejo-Barrera, P. Bermejo-Barrera, Multi-element determination in raft mussels by fast microwave-assisted acid leaching and inductively coupled plasma-optical emission spectrometry, Talanta 72 (2007) 1178–1185.
[30] A. Durand, Z. Chase, A.T. Townsend, T. Noble, E. Panietz, K. Goemann, Improved methodology for the microwave digestion of carbonate-rich environmental samples, Int. J. Environ. Anal. Chem. 96 (2016) 119–136.
[31] A. Sahuquillo, J.F. López-Sánchez, R. Rubio, G. Rauret, R.P. Thomas, C. M. Davidson, A.M. Ure, Use of a certified reference material for extractable trace metals to assess sources of uncertainty in the BCR three-stage sequential extraction procedure, Anal. Chim. Acta 382 (1999) 317–327.
[32] Ph Quevauviller, A. Ure, H. Muntau, B. Griepink, Improvement of analytical measurements within the BCR-Programme: single and sequential extraction procedures applied to soil and sediment analysis, Int. J. Environ. Anal. Chem. 51 (1993) 129–134.
[33] J.L. Todolí, J.M. Mermet, Acid interferences in atomic spectrometry: analyte signal effects and subsequent reduction, Spectrochim. Acta, Part B 54 (1999) 895–929.
[34] A.B.S. Silva, J.M. Higuera, C.E.M. Braz, R.C. Machado, A.R.A. Nogueira, Evaluation of different nebulizers performance on microwave-induced plasma optical emission spectrometry, Spectrochim. Acta, Part B 168 (2020) 105867.
[35] N. Chalyavi, P.S. Doidge, R.J.S. Morrison, G.B. Partridge, Fundamental studies of an atmospheric-pressure microwave plasma sustained in nitrogen for atomic emission spectrometry, J. Anal. At. Spectrom. 32 (2017) 1988–2002.
[36] K.J. Jankowski, E. Reszke, Microwave Induced Plasma Analytical Spectrometry, Royal Society of Chemistry, Cambridge, 2011.
[37] R. Serrano, G. Grindlay, P. Niedzielski, L. Gras, J. Mora, Evaluation of MIP-OES as a detector in DLLME procedures: application to Cd determination in water samples, J. Anal. At. Spectrom. 35 (2020) 1351–1359.
[38] A. Kramida, Yu Ralchenko, J. Reader, NIST ASD Team, NIST Atomic Spectra Database (Ver. 5.10), 2022 (Last access July 2023): https://physics.nist.gov/asd.
[39] R. Serrano, G. Grindlay, L. Gras, J. Mora, Insight into the origin of carbon matrix effects on the emission signal of atomic lines in inductively coupled plasma optical emission spectrometry, Spectrochim. Acta, Part B 177 (2021) 106070.
[40] E.V. Polyakova, O.V. Pelipasov, Plasma molecular species and matrix effects in the Hummer cavity microwave induced plasma optical emission spectrometry, Spectrochim. Acta, Part B 173 (2020) 105988.
[41] O.V. Pelipasov, E.V. Polyakova, Matrix effects in atmospheric pressure nitrogen microwave induced plasma optical emission spectrometry, J. Anal. At. Spectrom. 35 (2020) 1389–1394.
[42] K. Jankowski, K. Dreger, Study of an effect of easily ionizable elements on the excitation of 35 elements in an Ar-MIP system coupled with solution nebulization, J. Anal. Atomic Spectrom. 15 (2000) 269–274.
[43] G.C. Chan, G.M. Hieftje, Using matrix effects as a probe for the study of the charge-transfer mechanism in inductively coupled plasma-atomic emission spectrometry, Spectrochim. Acta, Part B 59 (2004) 163–183.
[44] S.A. Lehn, G.M. Hieftje, Experimental evaluation of analyte excitation mechanisms in the inductively coupled plasma, Spectrochim. Acta, Part B 58 (2003) 1821–1836.
[45] K. Wagatsuma, K. Satoh, Estimation using an enhancement factor on non local thermodynamic equilibrium behavior of high-lying energy levels of neutral atom in argon radio-frequency inductively-coupled plasma, Anal. Sci. 32 (2016) 535–541.
[46] R. Singh, Sisir Kumar Mitra, Scientific achievements and the fellowship of the royal society of London, Indian J. Hist. Sci. 52 (2017) 407–419.
[47] K.L. Lowery, T. McSweeney, S.P. Adhikari, A. Lachgar, G.L. Donati, Signal correction using molecular species to improve biodiesel analysis by microwave induced plasma optical emission spectrometry, Microchem. J. 129 (2016) 58–62.
[48] A.B.S. Silva, J.M. Higuera, A.R.A. Nogueira, Internal standardization and plasma molecular species: signal correction approaches for determination of phosphorus from phospholipids in meat by MIP-OES, J. Anal. At. Spectrom. 34 (2019) 782–787.
[49] L.N. Pires, F.S. Dias, L.S.G. Teixeira, Assessing the internal standardization of the direct milti-element determination in beer samples through microwave-induced plasma optical emission spectrometry, Anal. Chim. Acta 1090 (2019) 31–38.
[50] 2002/657/EC: Commission Decision of 12 August 2002 Implementing Council Directive 96/23/EC Concerning the Performance of Analytical Methods and the Interpretation of Results.
[51] Canadian Council of Ministers of the Environment, Guidance manual for environmental site characterization in support of environmental and human health risk assessment, Volume 4 Analytical Methods 1557 (2016). ISBN 978-1-77202-032-8.
[52] International Atomic Energy Agency, Soil Sampling for Environmental Contaminants, IAEA, Vienna, 2004. ISBN 92-0-111504-0.
[53] Environmental Protection Agency (EPA), EPA/600/R-96/055 Guidance for the Data Quality Objectives Process EPA QA/G-4, 1994.
[54] J. Inczédy, T. Lengyel, A.M. Ure, A. Gelencsér, A. Hulanicki, IUPAC Analytical Chemistry Division, Compendium of Analytical Nomenclature, third ed., Blackwell, Oxford, 1998.
[55] F.C. Jofré, D.N. Larregui, V.N. Murcia, P. Pacheco, M. Savio, Infrared assisted digestion used as a simple green sample preparation method for nutrient analysis of animal feed by microwave induced plasma atomic emission spectrometry, Talanta 231 (2021) 122376.
[56] M.S. Lemos, K.G.F. Dantas, Evaluation of the use of diluted formic acid in sample preparation for elemental determination in crustacean samples by MIP-OES, Biol. Trace Elem. Res. 201 (2023) 3513–3519.